



HAL
open science

Sensitivity of Microwave Interferometer in the Limiter Shadow to filaments in ASDEX upgrade

Mariia Usoltceva, Stéphane Heuraux, Ildar Khabibullin, Helmut Faugel,
Helmut Fünfgelder, Volodymyr Bobkov, Asdex Team

► **To cite this version:**

Mariia Usoltceva, Stéphane Heuraux, Ildar Khabibullin, Helmut Faugel, Helmut Fünfgelder, et al.. Sensitivity of Microwave Interferometer in the Limiter Shadow to filaments in ASDEX upgrade. Contributions to Plasma Physics, 2022, 10.1002/ctpp.202100194 . hal-03587168

HAL Id: hal-03587168

<https://hal.univ-lorraine.fr/hal-03587168>

Submitted on 24 Feb 2022

HAL is a multi-disciplinary open access archive for the deposit and dissemination of scientific research documents, whether they are published or not. The documents may come from teaching and research institutions in France or abroad, or from public or private research centers.

L'archive ouverte pluridisciplinaire **HAL**, est destinée au dépôt et à la diffusion de documents scientifiques de niveau recherche, publiés ou non, émanant des établissements d'enseignement et de recherche français ou étrangers, des laboratoires publics ou privés.

Sensitivity of Microwave Interferometer in the Limiter Shadow to filaments in ASDEX upgrade

Mariia Usoltceva¹ Stéphane Heuraux² Ildar Khabibullin³ Helmut Faugel¹

Helmut Fünfgelder¹ Volodymyr Bobkov¹ ASDEX Upgrade Team¹

¹Max-Planck-Institut für Plasmaphysik Garching , Germany

²Université de Lorraine, CNRS, Institut Jean Lamour , Nancy France

³Max-Planck-Institut für Astrophysik, Garching , Germany

Abstract

Microwave Interferometer in the Limiter Shadow (MILS) is a new diagnostic, installed on ASDEX Upgrade for electron density measurements in the far Scrape-Off Layer (SOL). At the chosen frequency of 47 GHz, the region of measurements varies within several centimetres before and after the limiter, depending on the density. 200 kHz bandwidth allows resolving transient events such as edge localized modes filaments and turbulence filaments. The measured quantities, phase shift, and power decay of the microwave beam, which crosses the plasma, are directly connected to the density and do not depend on any other plasma quantity. In this work, we analyse the influence of a filamentary perturbation on MILS signals. Simple representation of a filament is adopted, with parameters relevant to experimental filament properties, reported for ASDEX Upgrade. Forward modelling is done in COMSOL software by using RAPLICA-SOL, to study the response of the MILS synthetic diagnostic to the presence of a filament. Qualitative and quantitative dependencies are obtained and the boundaries of MILS sensitivity to filaments, or to the density perturbation in far SOL in general, are outlined.

KEYWORDS

density measurement, edge localized mode, filament, plasma diagnostic, Tokamak

1 | INTRODUCTION

In the Scrape-Off Layer (SOL) of a tokamak, the particle transport and the resulting density distribution are largely influenced (or often defined) by filaments. Such intermittent transport events can be large when associated with an edge localized mode (ELM) or small when they originate from the turbulence between ELMs or in an L-mode. Properties of filamentary transport have been a subject of an extensive research.^[1,2]

Microwave Interferometer in the Limiter Shadow (MILS)^[3] is a new diagnostic, installed on ASDEX Upgrade for electron density measurements in the far SOL. At the chosen frequency of 47 GHz, the radial span of measurements lies within several centimetres before and after the limiter. 200 kHz bandwidth allows resolving important transient plasma edge events. The measured quantities, phase shift, and power decay of the microwave beam, which crosses the plasma,

are directly connected to the density and, for the used well-aligned O-mode configuration, do not depend on any other plasma quantity.^[4]

Forward modelling is used for the reconstruction of the plasma density profile in far SOL from measured signals.^[3] This method is applicable to a monotonic inter-ELM-like density profile without large perturbations. In this work, we aim at studying the influence of the filament presence on the signals of MILS. Such description should be closer to experimental conditions, where turbulence and blobs are always present.

A simplified representation of the filaments is adopted in the current study, where they are defined as circular or bean-shaped structures, elongated along the field lines. By simulating filaments with various sizes and density levels, we explore the range of the detection of such structures and find correlations between the filament properties and the MILS signals of the synthetic diagnostic.

2 | EXPERIMENTAL AND SYNTHETIC DIAGNOSTICS

MILS consists of two microwave horn antennas, emitter and receiver, aligned and directed at each other, with 42.5 cm distance between them (Figure 1a). The axis of the interferometer is oriented perpendicularly to the background magnetic field and the wave at $f = 47$ GHz is sent in the O-mode polarization, making the measured signal sensitive to the density only.^[4]

In the synthetic diagnostic,^[3] the wave propagation is simulated in a limited region between the horns, where it matters for the received signal. The full-wave 3D modelling is done in COMSOL by using RAPLICASOL approach of wave propagation simulation in cold plasma^[5] (cold plasma approximation is valid for the SOL plasma conditions, where electron temperature is ≤ 100 eV), where absorbing material surrounds the plasma domain and ensures a single-pass absorption. Figure 1b shows the radial-poloidal cross-section of the simulation domain with an example of wave propagation in plasma with density exponentially increasing towards the core, as described in details in Ref. [3]. The core plasma is on the left, with the flux surfaces approximated by circles concentric to the circle that defines the limiter. The coordinate system in the model is defined as follows: z -axis is aligned with the background magnetic field, y -axis is aligned with the MILS axis, which is tangential to plasma, and therefore, the x -axis points in the radial direction.

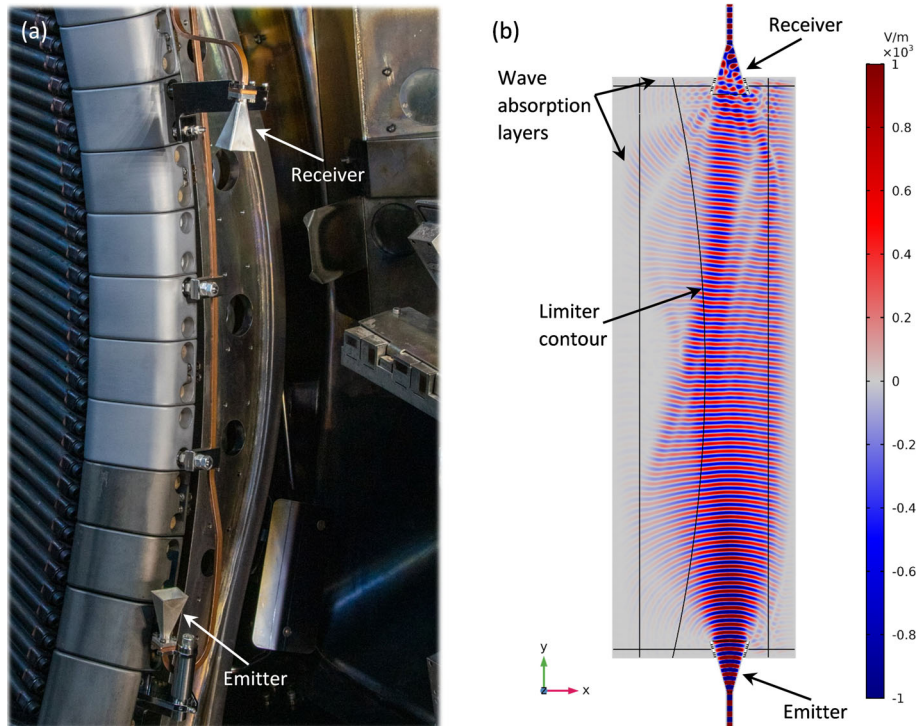


FIGURE 1 (a) Microwave Interferometer in the Limiter Shadow (MILS) experimental setup, (b) MILS synthetic diagnostic setup

In the field-aligned direction (z), the horn antennas of MILS have the size of 2 cm. The signal is, therefore, collected from a very thin region of the same size. On such scale, we can assume the variation of plasma density along the field lines as negligible. No reflections or refractions in the y - z plane, which could influence the collected signal, are expected.

When considering the wave propagation in the radial-poloidal (x - y) plane, part of the beam, which goes towards the high-density plasma, gets refracted and is able to reach the receiver (Figure 1b). The span of the radial density profile, which has influence on the collected signal, therefore, is much larger than the horn radial size. The signal is, therefore, collected from a large volume; it experiences interference inside the receiver horn and converts into the waveguide fundamental mode, which propagates to the detecting hardware. The previous study of the measurement region of MILS shows that the part of the radial density profile (for monotonic profiles), which influences the MILS measurements, has a length of ~ 5 cm and is located near the limiter edge, more towards the core plasma for lower densities and towards outside for higher densities.^[3]

3 | MODEL VERIFICATION

In previous work, we have verified the correct functioning of the model, that is, sufficient resolution, solver correctness, and error-free parameters definition, by comparing the numerical results to theoretical predictions for some simple cases of plasma density.^[3] Here we also perform a simple check in order to ensure that the density perturbations with large gradients over small distances can be sufficiently resolved.

For this test, the density inside the plasma volume is defined as a sum of two contributions $n_e = n_{bg} + n_{ptb}(y)$. To a constant density background of $n_{bg} = 0.5 \times 10^{18} \text{ m}^{-3}$, in each model, a perturbation of density $n_{ptb}(y)$ along y -direction is added. The density along x and z does not vary. The perturbation has a shape of a narrow Gaussian peak in the middle of MILS axis: $n_{ptb}(y) = n_{flm} * \exp\left(-\frac{y^2}{2\sigma^2}\right)$. The peak density n_{flm} and the size $\sigma = \text{FWHM}/(2\sqrt{2 * \log(2)})$ (FWHM—full width at half maximum) of the perturbation are varied. For this test and for further studies, we choose these parameters in the range within the typical filament characteristics reported from experimental data.^[6-8]

The phase shift can be calculated theoretically from the following formula (explained in detail in Ref. [9]):

$$\Delta\varphi = \frac{2\pi d}{\lambda_{vac}} \left(1 - \frac{1}{d} \int_0^d N(x) dx \right) = \frac{2\pi d}{\lambda_{vac}} \left(1 - \frac{1}{d} \int_0^d \sqrt{1 - \frac{\omega_p^2}{\omega^2}} dx \right), \quad (1)$$

where d is the MILS axis length, λ_{vac} is the wavelength in vacuum, $N = 1 - \frac{\omega_p^2}{\omega^2}$ is the refractive index as defined for O-mode, $\omega = 2\pi f$ is the angular frequency of the wave, $\omega_p = \sqrt{\frac{e^2 n_e}{\epsilon_0 m_e}}$ is the electron plasma frequency, e is the electron charge, m_e is the electron mass, and ϵ_0 is the vacuum permittivity. $n_c = \frac{\epsilon_0 m_e \omega^2}{e^2}$ is the cut-off density, which can be used to rewrite Equation (1):

$$\Delta\varphi = \frac{2\pi d}{\lambda_{vac}} \left(1 - \frac{1}{d} \int_0^d \sqrt{1 - \frac{\left(n_{bg} + n_{flm} * \exp\left(-\frac{y^2}{2\sigma^2}\right) \right)}{n_c}} dx \right). \quad (2)$$

The integration of Equation (2) is done numerically, since there is no analytical expression for this integral. The theoretical values are compared to the simulation results (Figure 2a). The mean deviation from the theory is 0.035° and the maximum deviation is 0.22° (at $n_{flm} = 1.5 \times 10^{18} \text{ m}^{-3}$, FWHM = 3 cm), which means that the numerical errors are extremely low.

A second test is done with a 2D Gaussian perturbation, located at $x = 0$ and $y = 0$ m, that is, in the middle between the MILS antennas. The density along z is constant. The modelling results are compared with theoretical calculation done with the same Equation (1) and a large deviation is observed for nearly all points (Figure 2b). The discrepancy is caused by the fact that in this case, only a part of the detected beam passes through the maximum of the perturbation (along the MILS axis), while some rays only go through the periphery of the filament and experience lower phase shift. The largest discrepancy is observed for the smallest filament size, where this effect is the most significant. It was noticed that for the

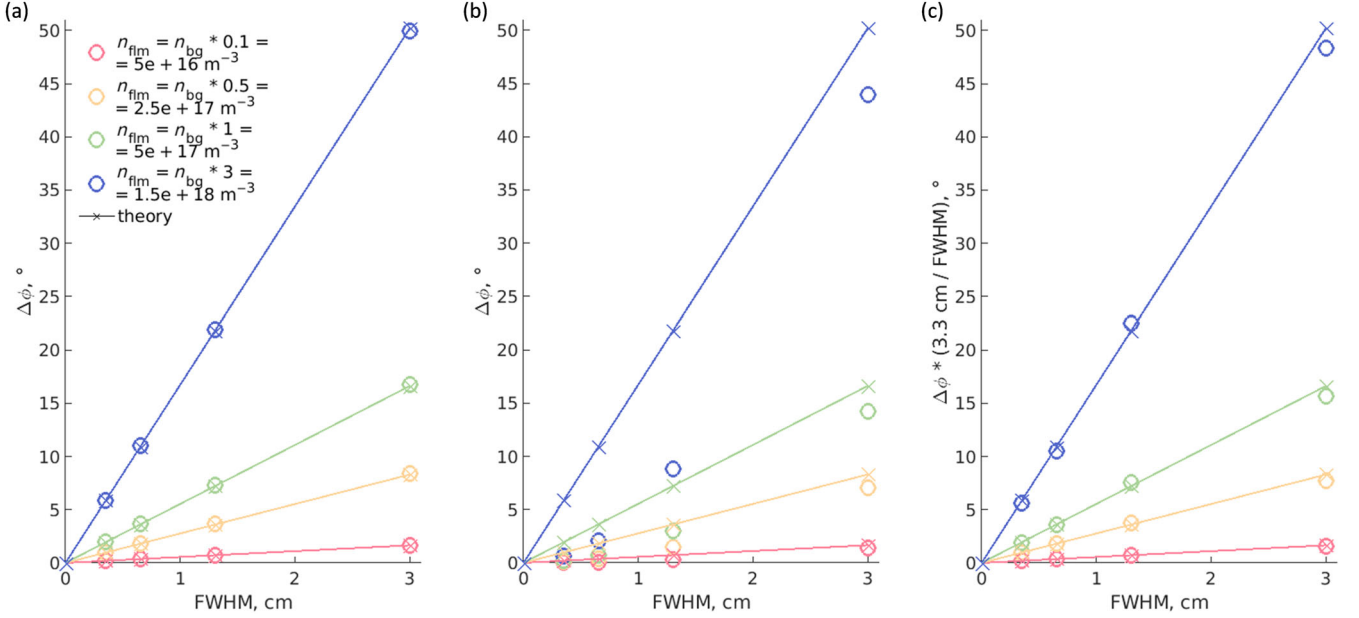


FIGURE 2 (a) Numerical and theoretical calculation of phase shift caused by a 1D Gaussian density perturbation along Microwave Interferometer in the Limiter Shadow (MILS) axis. (b,c) Numerical and theoretical calculation of phase shift caused by a 2D circular filament: (b) phase shift, (c) normalized phase shift, see Equation (3)

considered filament shape and for constant background plasma density, the deviation of the phase from the theoretical prediction due to the size of the filament is inversely proportional to the filament size. A coefficient of 3.3 cm can be chosen to normalize the obtained phase value (representing a radial stretch of a filament, sufficient to cause a full phase shift of the whole collected beam), good matching to the theory can be restored (Figure 2c):

$$\Delta\phi_{\text{norm}} = \Delta\phi * \frac{3.3 \text{ cm}}{\text{FWHM}}. \quad (3)$$

The found dependence should not be generalized to the cases of arbitrary filament shape and arbitrary background plasma density distribution and, therefore, it is mostly useful for basic validations of the numerical model.

The successful model verification with the described tests allows us to use the model for further studies and to estimate the numerical errors. Density profiles with perturbations of small size and large amplitude, resulting locally in high gradients of density, can be sufficiently resolved in the employed model. The maximum numerical error for phase calculation observed in the tests is below 0.5° , which means it is within the total random error of our model evaluated in Ref. [3].

4 | MODELLING OF FILAMENT PROPAGATION

In this section, we consider a simplified description of a filament-like structure propagating in the SOL. The background density is defined as a monotonic exponentially decreasing density profile same as in Ref. [3], described by three parameters ($n_{\text{lim}}, a_{\text{in}}, a_{\text{out}}$): $n_{\text{bg}} = n_{\text{lim}} * \exp(a * x)$, where n_{lim} is the density at the limiter and a is the inversed decay length, different for the plasma in front of the limiter $a = a_{\text{in}}$ and in the Limiter Shadow $a = a_{\text{out}}$.

A filamentary perturbation is added to the background, with the following simplifying assumptions:

- a single filament is considered
- no poloidal velocity, only radial propagation
- no variation of background and filament density along z (toroidally), in 2 cm wide measurement region
- circular or bean-shape x - y cross-section

- 2D Gaussian distribution of filament density
- filament density either constant or exponentially decreasing when radially moved
- far from the separatrix, because in its vicinity an ELM perturbation of density looks less similar to a filament.^[6]

While the real filaments can deviate from the adopted assumptions, we want to qualitatively reproduce such type of density perturbation and analyse the sensitivity of MILS to it. Large filaments can be relevant to experimental conditions during a type-I ELM, while smaller ones would be closer to small ELMs or inter-ELM filaments.

From experimental observations, it is expected that the filament density decreases when the filament moves radially outwards.^[10] The two considered cases are the lower (constant density) and the upper (density decaying with the same decay length as the decay length of the background plasma density) boundaries for the filament density decay during radial movement. Some experimental observations point out that the filament radial-poloidal cross-section should look less like a circle and more bean-shaped, that is, elongated along the flux surfaces^[8]; similar shape is observed in ELMs simulations.^[11] Therefore, we consider both a circular and a bean-shaped cross-sections.

4.1 | Filament with radially constant density

In this test, a filament is moved radially and its density stays constant at all radial positions. It leads to the filamentary distortion being insignificant at the locations with high background density. Therefore, the radial range of the filament detection can differ depending on the background density profile and on the density of the filament itself. A scan of the filament density and size, as well as of the background density profile, is performed, in order to find systematic dependencies.

In Figure 3, the phase-power diagram of MILS synthetic diagnostic output is shown. The phase variation $\Delta\varphi$ corresponds to the change of the phase difference between the receiver and the emitter in plasma relative to the phase difference measured in vacuum: $\Delta\varphi = (\varphi_{\text{rec}} - \varphi_{\text{emit}})_{\text{pl}} - (\varphi_{\text{rec}} - \varphi_{\text{emit}})_{\text{vac}}$. The power change P/P_{vac} represents the detected power at the receiver relative to the power detected in vacuum: $P/P_{\text{vac}} = (P_{\text{rec}})_{\text{pl}} / (P_{\text{rec}})_{\text{vac}}$, while the emitter power always stays the same and does not influence this ratio. The database, constructed with monotonic density profiles,^[3] is shown with points in grey. Each point corresponds to phase and power measured by the synthetic diagnostic for one monotonic density profile, and the database covers the variety of density values, expected in ASDEX Upgrade. Several points of the database (with corresponding density profile parameters indicated on the plot) serve as starting points for this study and each trajectory of a filament starts from such a point. Arrows show the filament propagation from negative to positive x , that is, towards the wall. We consider the filament as “detected,” when the phase and power values lie outside of the error bar region of the initial point, 1° and 3% for phase and power, respectively. For each filament, the detection region is given in the plot legend.

Four examples are given (in blue in Figure 3a) of a filament with the same characteristics, which propagates through plasma with different background density. Their trajectories in the phase-power space have slightly similar shapes and all exhibit quite large deviation from their initial points. The same can be seen in Figure 3b for the case of a smaller filament and this tendency was noticed in all studied cases. When trajectories starting from the same point are considered, it can be observed that they repeat exactly the same shape, while the size of the trajectory scales with the filament density.

It is also possible to establish quantitative correlations between the filament properties and the MILS signal variation. In Figure 4, the maximum deviations of $\Delta\varphi$ and P/P_{vac} from the initial point are plotted as functions of the filament integral density $n_{\text{intg}} = \text{FWHM} * n_{\text{film}}$. There is a clear correlation (linear in logarithmic scale) for both phase and power, with the approximation functions $\log_{10} \Delta\varphi_{\text{dev}} = 1.434 * \left(\log_{10} \frac{n_{\text{intg}}}{10^{18}} + 0.41 \right)$ and $\log_{10} P/P_{\text{vac,dev}} = 1.186 * \left(\log_{10} \frac{n_{\text{intg}}}{10^{18}} + 0.78 \right)$, respectively. From the same plot, the limits of the filament detection can be derived, in terms of integral density. For a given lower limit on the detectable phase and power deviation ($\Delta\varphi = 1^\circ$ and $P/P_{\text{vac}} = 3\%$ are taken as an example), the minimum detectable filament integral density can be obtained ($\approx 3 \times 10^{17} \text{ cm m}^{-3}$ in this example).

4.2 | Filament with radially decaying density

Another study has been done, where the same circular-shaped filament is tracked during the same radial movement, but the density of the filament changes at each radial step. Its density is proportional to the background density at each point, so the filament density decay length is the same as that of the background plasma density.

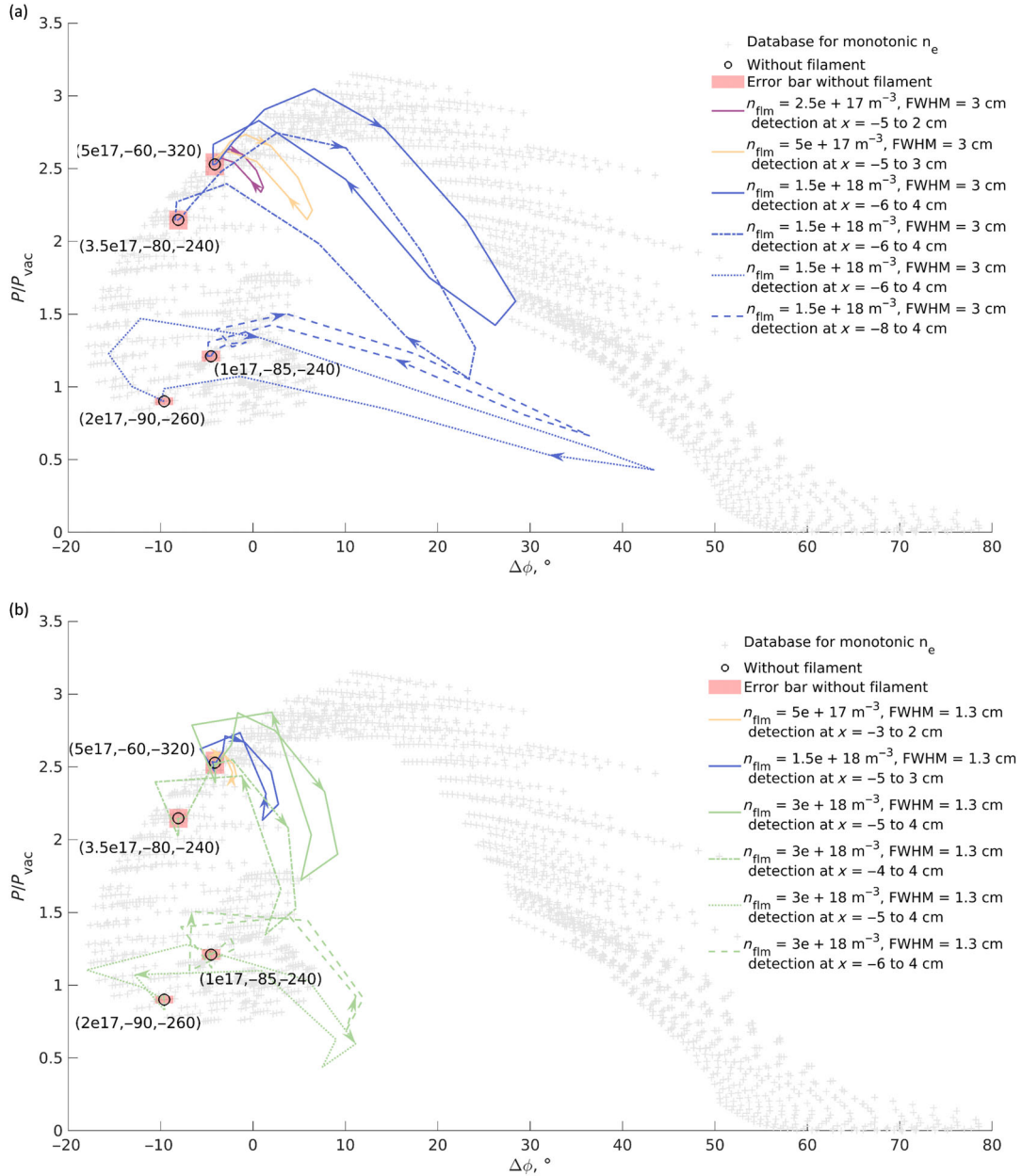


FIGURE 3 Phase-power diagram with points from monotonic density database plotted in the background, some of which are the starting points of tests with a filament, labelled with their density profile in the format $(n_{lim}, a_{in}, a_{out})$. Influence of a filament presence is shown as a trajectory; arrows show the filament movement from dense plasma to the edge. Detection range along x is given for each filament ($x = 0$ cm is the Microwave Interferometer in the Limiter Shadow (MILS) axis). (a) Larger and (b) smaller filament is taken. This figure is for filaments with constant density at each radial position

Results of the simulations are shown in Figure 5 in the same way as in the previous subsection. Large qualitative differences can be seen in the shapes of the trajectories compared to Figure 3. It means that on the qualitative level we are able to distinguish the two used theoretical descriptions of the filament propagation.

When comparing trajectories for the same filament but different background density, some similarities can be observed, though less pronounced than for the cases in Section 4.1. There is no exact shape preservation for the trajectories starting from the same point and corresponding to different filament density, only a general similarity. The amplitude of phase and power deviation is proportional to the filament density (and to the filament size as well).

As in Section 4.1, the same linear in the logarithmic scale correlation is observed between the maximum deviation of the phase and power and the integral density of the filament, with the approximation functions $\log_{10} \Delta\phi_{dev} = 0.675 *$

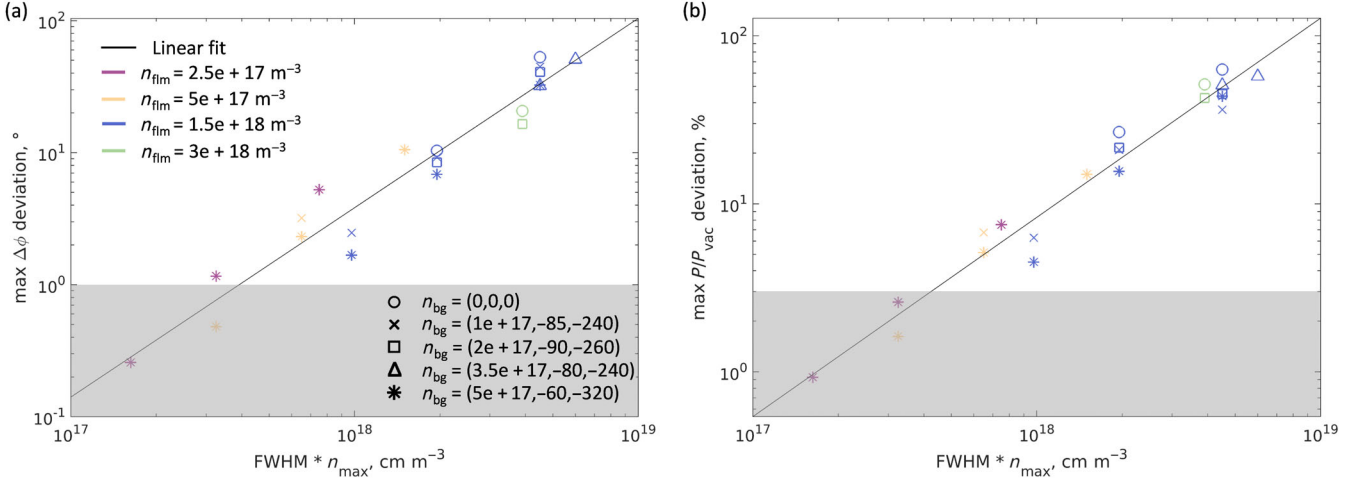


FIGURE 4 Correlation of the (a) phase and (b) power maximum deviation with the filament integral density. The shaded area illustrates an example of the border of the filament detection

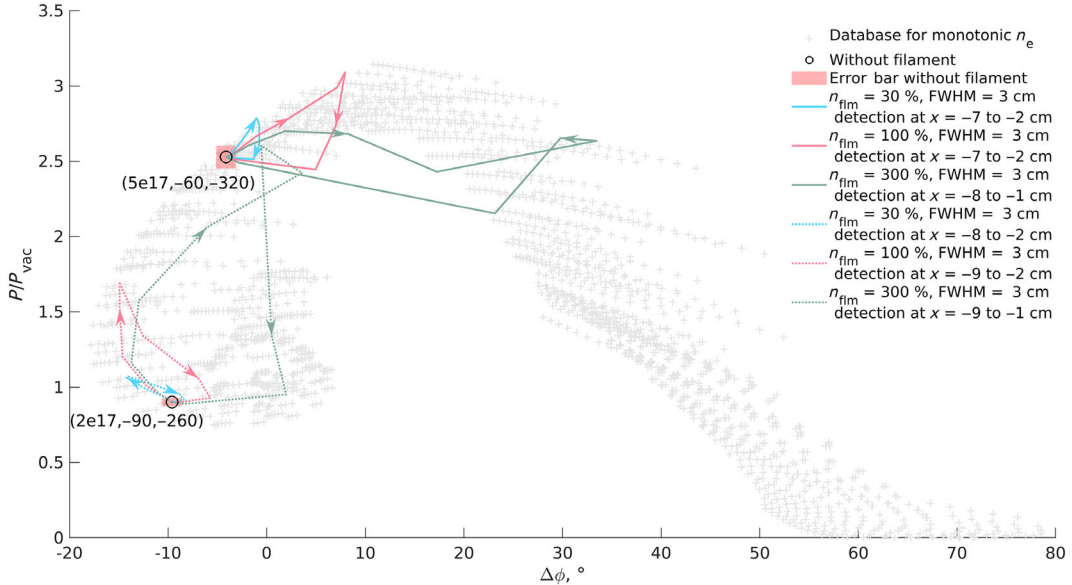


FIGURE 5 Examples of filaments with density decaying with radial position (phase-power diagram as in Figure 3)

$\left(\log_{10} \frac{n_{\text{intg}}}{10^{18}} + 0.51\right)$ and $\log_{10} P/P_{\text{vac,dev}} = 1.279 * \left(\log_{10} \frac{n_{\text{intg}}}{10^{18}} + 0.10\right)$, respectively. Different from the previous case, the typical radial location of the filament, when it introduces the largest perturbation to MILS measurements, is not in the Limiter Shadow. For a filament of constant density, the maximum is almost always at $x = 0$ cm, that is, at the MILS axis. It is explained by the fact that such filament becomes prominent only when it reaches the radial position with quite low background density and it affects the MILS signal the most when located at MILS axis. For a filament with radially decreasing density, the location of maximum perturbation is shifted towards the core plasma, with the mean value at $x = -4.5$ cm, that is, at 2.5 cm in front of the limiter. Such filament, when moved further to low-density plasma, becomes less dense itself and causes weaker change in the signal of MILS.

4.3 | Circular filament and filament elongated poloidally

We compare the impact of a circular filament and of a filament with a cross-section shape elongated along the flux surfaces (poloidally), shown in Figure 6. The density distribution of the elongated filament is defined by the function:

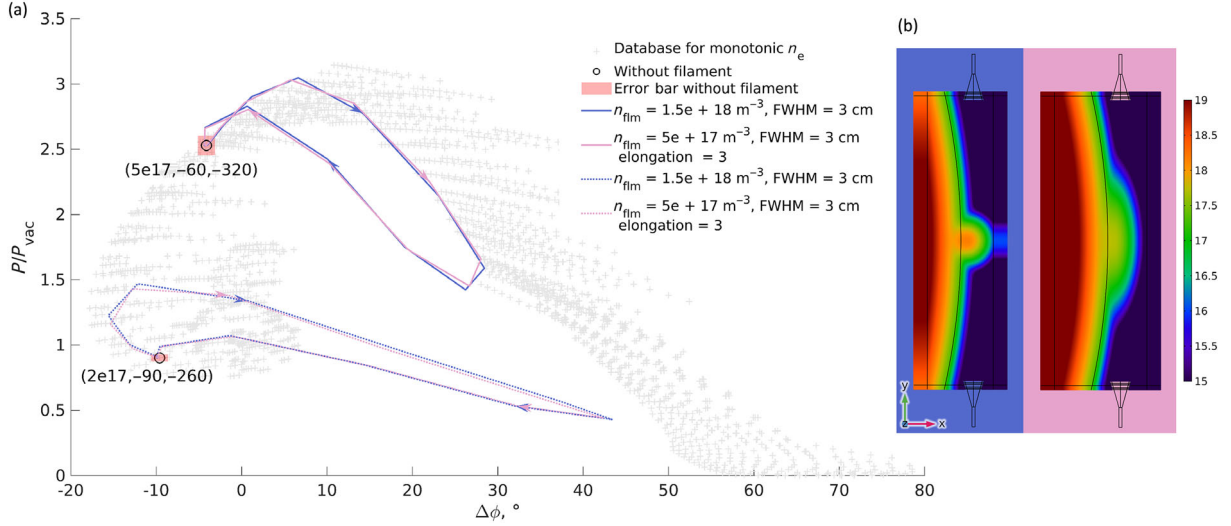


FIGURE 6 (a) Comparison of circular and poloidally elongated filaments (phase-power diagram as in Figure 3). (b) 2D density profiles with circular and poloidally elongated filament shape, with the plot background colour corresponding to the trajectory colour

$$n_{\text{fil}}(x, y) = n_{\text{max}} * \exp\left(-\frac{(R - R_0)^2}{2\sigma_r^2}\right) * \exp\left(-\left(a \sin \frac{y}{R_0} - a \sin \frac{y_0}{R_0}\right)^2 * \frac{R_0^2}{2(\varepsilon * \sigma_r)^2}\right), \quad (4)$$

where the coordinates x, y are defined differently from their previous usage, they have zero at the centre of the concentric circles of constant density, approximating the flux surfaces; $R = \sqrt{x^2 + y^2}$, $R_0 = \sqrt{x_0^2 + y_0^2}$, x_0 and y_0 are the coordinates of the filament centre, ε is the elongation, and σ_r relates to the radial size of the filament.

For relatively low (experimentally relevant—see Ref. [8]) values of the ratio between the radial and the poloidal size, the trajectory of an elongated filament repeats nearly exactly the trajectory of a circular filament with the same integral density along y (Figure 6). It happens because the direction of MILS beam propagation is not very different from the directional of poloidal elongation and of the y -direction, because both the refracted beam and the flux surfaces have moderate curvature. With elongation ratio $\gg 1$, it would not be the same, because the beam would not pass through the filament centre along its whole extension.

5 | SENSITIVITY OF FILAMENT DETECTION TO ITS LOCATION

The tests in Section 4 have been done with a filament moving radially in the middle between the MILS antennas. It is useful to explore the spatial limit of a filament detection in a larger range of its location. Figure 7 show the results of an analysis for one case of the background density ($0.5e18, -60, -320$), with filament size $\text{FWHM} = 3$ cm. Both types of filaments are considered, with radially decaying density $n_{\text{fil}} = 100\%$ of the background density (Figure 7a,b) and with constant density $0.5e18 \text{ m}^{-3}$ at each radial point (Figure 7c,d). When other values are taken for the background plasma and filament properties, the detection area would be different but qualitatively similar. In the plots, empty circles show the points where the values are below the chosen detection limit, 1° and 3% for phase and power, respectively. If the experimental conditions (noise, plasma turbulence, etc.) set this limit higher, the detection area would shrink noticeably in y direction and in x -direction as well.

The results for two types of filaments are quite different. The filament with density proportional to the background density (Figure 7a,b) has the largest impact on the signal at ~ 2 cm in front of the limiter, in the middle of the MILS axis. There is a strong reduction of the signal perturbation at locations further away from $y = 0$ cm. For the chosen values of the background plasma density and the filament density, the filament does not have large enough density in the Limiter Shadow to make a noticeable impact on the collected signal.

The opposite is true for a filament with constant density (Figure 7c,d). In the region where the background density is significantly decreased (mostly in the Limiter Shadow), the filament influences considerably the wave propagation. At

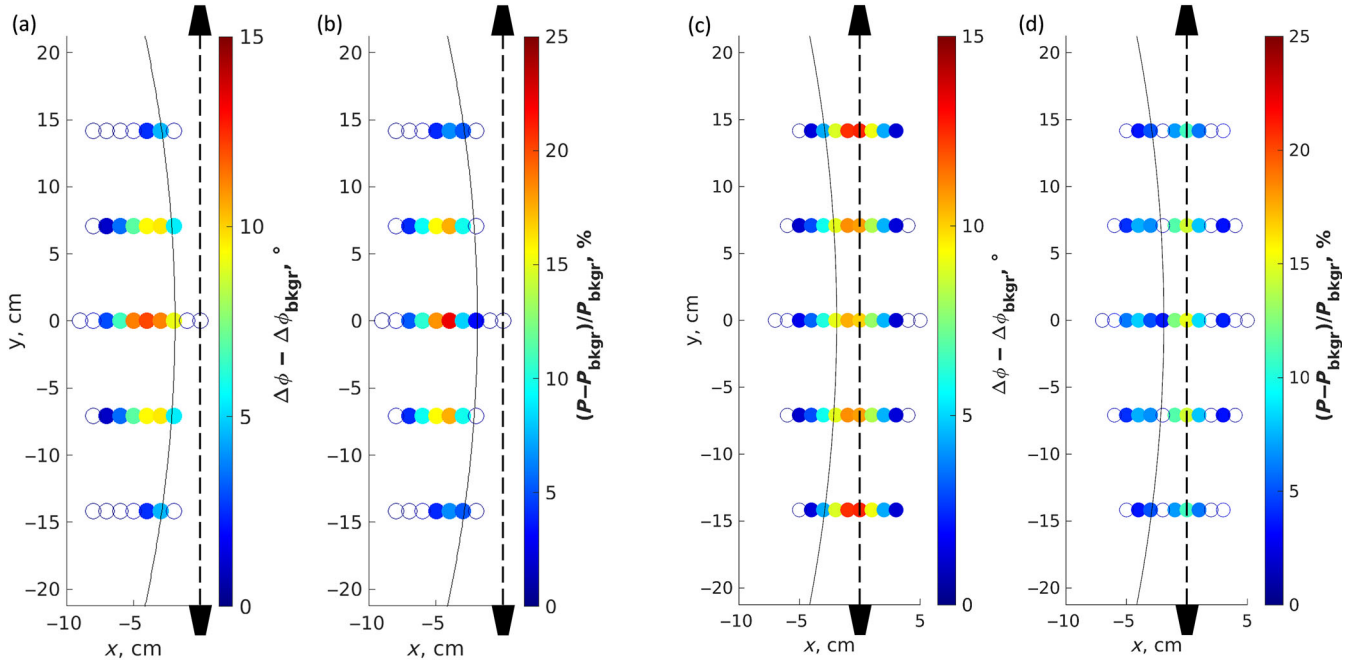


FIGURE 7 Examples of spatial boundaries of a filament detection by a change in (a), (c) phase and (b), (d) power, for (a), (b) filament with radially exponentially decreasing density and (c), (d) filament with radially constant density. Empty circles have values below the detection limit of 1° and 3% for phase and power, correspondingly. Microwave Interferometer in the Limiter Shadow (MILS) antennas and axis and the limiter contour are schematically shown

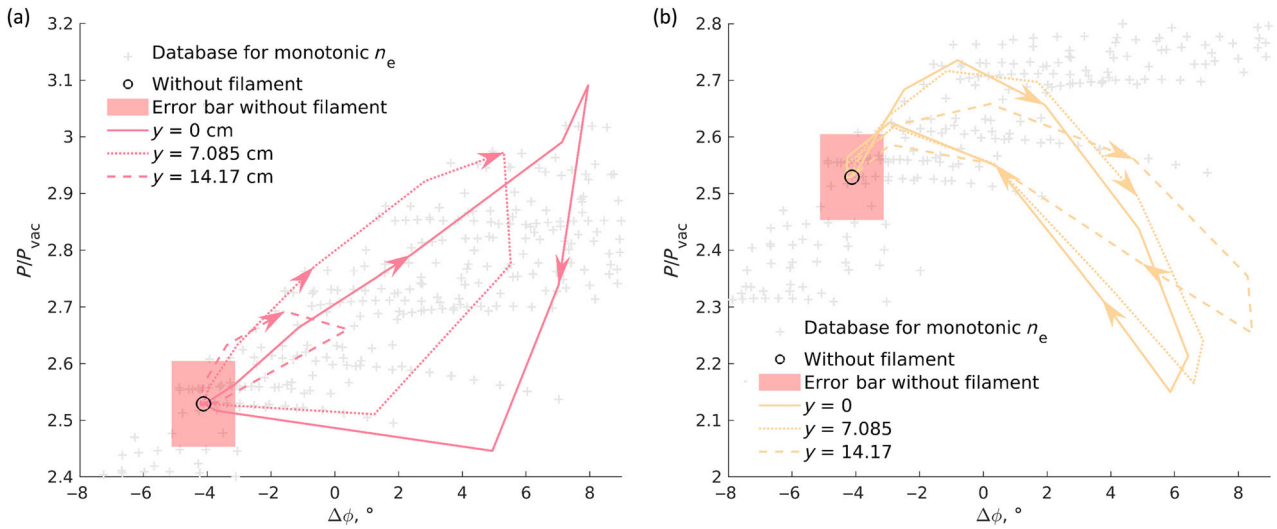


FIGURE 8 Trajectories of a filament propagating radially at different y values (identical at negative y , therefore, not plotted), for (a) filament with radially exponentially decreasing density and (b) filament with radially constant density

different positions along y -axis, the change in phase and power has almost the same pattern, since the filament density is the same. As was noted before, the two considered cases are the two extremities of the filament behaviour. The actual detection area should be somewhere in between these two results.

The shape of the trajectory of a filamentary density perturbation in the phase-power diagram changes when the radial propagation at $y \neq 0$ is considered (Figure 8). However, it is still quite close to the case $y = 0$ and it does not change strongly enough to not be distinguished from other shapes, for example, between the two types of filament radial density change, as in Figure 8a,b.

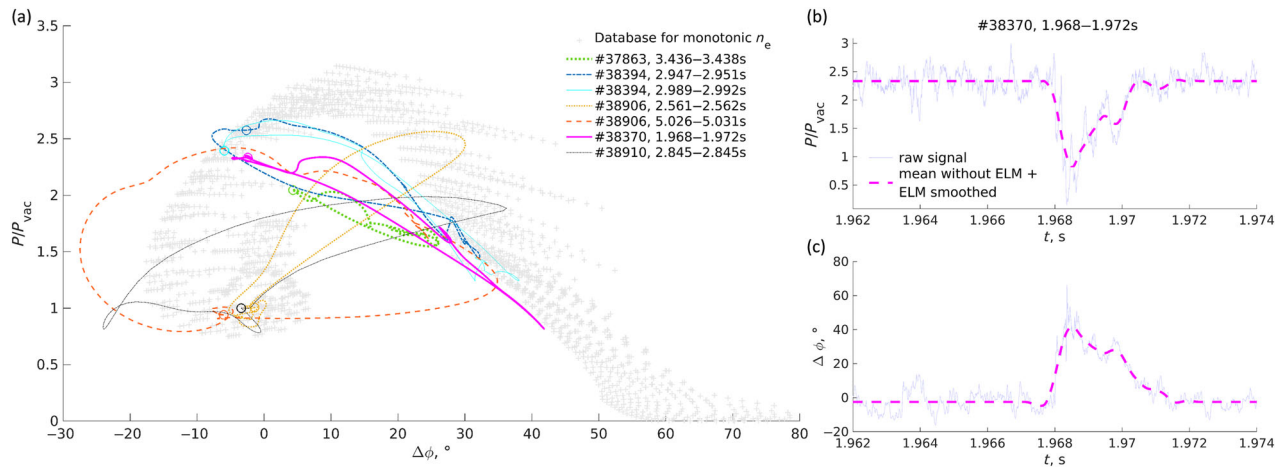


FIGURE 9 (a) Examples of experimental Microwave Interferometer in the Limiter Shadow (MILES) signals during edge localized mode (ELM) filaments in ASDEX Upgrade. Time evolution of (b) power and (c) phase signals for one of the examples in (a), with inter-ELM periods before and after the ELM

6 | EXPERIMENTAL EXAMPLES OF ELMS

In experiments on ASDEX Upgrade, the bandwidth of 200 kHz allows resolving the temporal evolution of the signal perturbation, caused both by ELMs and by smaller filaments. Examples of such perturbations for the case of ELM filaments, presented in the same way as the modelling results—as trajectories in the phase-power diagram, are shown in Figure 9a. Many curves resemble the trajectories in Figure 3, while some look as a case in between the shapes from Figures 3 and 5. These qualitative comparisons indicate, which theoretical description of the filament density variation during the radial propagation shows results closer to the experimental measurements of MILES. The exponential decay of the filament density with the same decay length as of the background density, used for the results in Figure 5, seems to be an over-estimation. The model with filament density staying constant or an option in between the two considered models, with slower filament density decay, agree better with the considered experimental data for ELMs.

From Figure 9b,c it can be seen that the level of density perturbation by the turbulence and small filaments is low enough for the meaningful calculation of the background mean values and the ELM signals. This example is taken as representative of the typical level of such perturbations, but examples with much lower or much higher perturbations also exist in the MILES data.

From the performed modelling, it can be estimated that the filament is detected along ~ 10 cm radial distance. When this value is divided by the duration of the MILES signal perturbation in experimental data, ~ 1 – 2 ms (for the examples of smaller ELMs, corresponding approximately to the simulated filaments), the filament radial velocity can be derived, resulting in ~ 50 – 100 m/s. While a lot of literature reports, higher ELM radial velocities,^[8] such results are mostly given for the velocity at the separatrix and in the near SOL. In the far SOL, the velocity of ELM filaments and turbulence filaments was observed to decrease.^[6,10]

More advanced analysis is required to make improved comparisons between the experiment and the theories. The presented study does not cover the filaments, which have non-negligible poloidal velocity. Their analysis will have an influence both on the interpretation of the shape of the filament trajectory in the phase-power diagram with respect to theories describing its properties and on the evaluation of the filament velocity components. The current study is limited to the qualitative investigation of MILES sensitivity to filaments, and the refined comparison to the experiment is foreseen in the future work.

7 | CONCLUSIONS

Filamentary perturbations of density in the far SOL are typical for experimental tokamak conditions. MILES, as a diagnostic aimed at density measurements in that region, is capable of detecting the density oscillations with high temporal resolution. For the interpretation of the observed oscillations, it is essential to study how a filamentary perturbation affects

the MILS signals. In this paper that question is examined by using basic theoretical descriptions of a single filament in the far SOL.

The performed analysis helps to outline the boundaries of the filament detection by MILS for the filament size, density, and poloidal-radial location. Qualitative features like the trajectory of the filamentary perturbation signal in the phase-power diagram can be associated with some characteristic assumptions used in the theoretical definition of the simulated density perturbation. Quantitative values can be obtained from the derived scaling's of the measured quantities, phase, and power, with the integral density of a filament. The velocity of the filament (only filaments with dominant radial velocity component are considered in this study) is indicated by the duration of the MILS signal perturbation, with the typical travelled length in the field of view of the diagnostic estimated from modelling.

This work also displays the sensitivity of MILS to the density perturbation in far SOL in general, since a single filament and a turbulent structure distributed along the whole MILS path can have similar influence on the measured signal. The integral value of the density perturbation can be estimated by the level of MILS signal oscillation from the found scaling's.

MILS synthetic diagnostic can utilize any 3D density distribution as an input, for example, from another modelling or from the experiment. With such forward modelling, it can be possible to study numerically and validate experimentally more advanced theories of density perturbation and turbulence in far SOL.

ACKNOWLEDGEMENTS

This work has been carried out within the framework of the French Federation for Magnetic Fusion Studies (FR-FCM) and EUROfusion Consortium and has received funding from the Euratom research and training programme 2014–2018 and 2019–2020 under Grant agreement No. 633053. The views and opinions expressed herein do not necessarily reflect those of the European Commission. Open Access funding enabled and organized by Projekt DEAL.

DATA AVAILABILITY STATEMENT

The data that support the findings of this study are available from the corresponding author upon reasonable request.

REFERENCES

- [1] D. Carralero, M. Siccinio, M. Komm, S. A. Artene, F. A. D'Isa, J. Adamek, L. Aho-Mantila, G. Birkenmeier, M. Brix, G. Fuchert, M. Groth, T. Lunt, P. Manz, J. Madsen, S. Marsen, H. W. Müller, U. Stroth, H. J. Sun, N. Vianello, M. Wischmeier, E. Wolfrum, *Nucl. Fusion* **2017**, *57*, 056044.
- [2] V. Naulin, *J. Nucl. Mater.* **2007**, *363-365*, 24.
- [3] M. Usoltceva, S. Heurax, I. Khabibullin, H. Faugel, *Rev. Sci. Instrum.* **2022**, *93*, 013502. <https://doi.org/10.1063/5.0074838>
- [4] T. H. Stix, *AIP "Waves in plasma"*, second ed. American Institute of Physics, New York, **1992**.
- [5] J. Jacquot, L. Colas, F. Clairet, M. Goniche, S. Heurax, J. Hillairet, G. Lombard, D. Milanese, *Plasma Phys. Control. Fusion* **2013**, *55*, 115004.
- [6] G. Fuchert, G. Birkenmeier, D. Carralero, T. Lunt, P. Manz, H. W. Müller, B. Nold, M. Ramisch, V. Rohde, U. Stroth, *Plasma Phys. Control. Fusion* **2014**, *56*, 125001.
- [7] G. T. A. Huijsmans, C. S. Chang, N. Ferraro, L. Sugiyama, F. Waelbroeck, X. Q. Xu, A. Loarte, S. Futatani, *Phys. Plasmas* **2015**, *22*, 218.
- [8] B. Lipschultz, X. Bonnin, G. Counsell, A. Kallenbach, A. Kukushkin, K. Krieger, A. Leonard, A. Loarte, R. Neu, R. A. Pitts, T. Rognien, J. Roth, C. Skinner, J. L. Terry, E. Tsitroni, D. Whyte, S. Zweben, N. Asakura, D. Coster, R. Doerner, R. Dux, G. Federici, M. Fenstermacher, W. Fundamenski, P. Ghendrih, A. Herrmann, J. Hu, S. Krasheninnikov, G. Kirnev, A. Kreter, V. Kurnaev, B. LaBombard, S. Lisgo, T. Nakano, N. Ohno, H. D. Pacher, J. Paley, Y. Pan, G. Pautasso, V. Philipps, V. Rohde, D. Rudakov, P. Stangeby, S. Takamura, T. Tanabe, Y. Yang, S. Zhu, *Nucl. Fusion* **2007**, *47*, 1189.
- [9] C. A. J. Hugenholtz, *Technische Universiteit Eindhoven, PhD Thesis* **1990**.
- [10] J. A. Boedo, D. L. Rudakov, E. Hollmann, D. S. Gray, K. H. Burrell, R. A. Moyer, G. R. McKee, R. Fonck, P. C. Stangeby, T. E. Evans, P. B. Snyder, A. W. Leonard, M. A. Mahdavi, M. J. Schaffer, W. P. West, M. E. Fenstermacher, M. Groth, S. L. Allen, C. Lasnier, G. D. Porter, N. S. Wolf, R. J. Colchin, L. Zeng, G. Wang, J. G. Watkins, T. Takahashi, The DIII-D Team, *Phys. Plasmas* **2005**, *12*, 072516.
- [11] M. Hoelzl, G. T. A. Huijsmans, S. J. P. Pamela, M. Bécoulet, E. Nardon, F. J. Artola, B. Nkonga, C. V. Atanasiu, V. Bandaru, A. Bhole, D. Bonfiglio, A. Cathey, O. Czarny, A. Dvornova, T. Fehér, A. Fil, E. Franck, S. Futatani, M. Gruca, H. Guillard, J. W. Haverkort, I. Holod, D. Hu, S. K. Kim, S. Q. Korving, L. Kos, I. Krebs, L. Kripner, G. Latu, F. Liu, P. Merkel, D. Meshcheriakov, V. Mitterauer, S. Mochalsky, J. A. Morales, R. Nies, N. Nikulsin, F. Orain, J. Pratt, R. Ramasamy, P. Ramet, C. Reux, K. Särkimäki, N. Schwarz, P. Singh Verma, S. F. Smith, C. Sommariva, E. Strumberger, D. C. van Vugt, M. Verbeek, E. Westerhof, F. Wiescholke, J. Zielinski, *Nucl. Fusion* **2021**, *61*, 065001.